APEM journal
Advances in Production Engineering & Management
Volume 15 | Number 3 | September 2020 | pp 295–306
https://doi.org/10.14743/apem2020.3.366
ISSN 1854-6250
Journal home: apem-journal.org
Original scientific paper

Computational analysis of cavitation at the tongue of the volute of a centrifugal pump at overload conditions

Hu, Q.[a], **Yang, Y.**[a], **Cao, W.**[a,*]

[a]Research Institute of Fluid Engineering Equipment Technology, Jiangsu University, P.R. China

ABSTRACT

Volute pump is the most common used centrifugal pump. As cavitation highly contributes to deteriorating the performance of the pump, anti-cavitation performance is one of its design specifications. To clarify the cavitation evolution at the tongue of the volute of a centrifugal pump at overload conditions and its influence on the flow field in the impeller, numerical simulation with ANSYS CFD and a hydraulic test were conducted on a volute pump at several flow rates above optimal value. The cavity distribution and the blade loading distribution were analyzed. And the characteristics of the pressure fluctuation of the monitoring points located in volute casing were obtained and compared with each other. Results showed that cavitation may first emerge at the tongue rather than the impeller inlet at overload conditions. The alternative stress resulting from periodical radial force increases obviously as the extent of cavitation at the tongue. Meanwhile, the mean cavity length grows as each blade comes close to the tongue, and causes a decrease in performance because of a reduction or closure of flow passages. The pressure pulsation in the volute is consistent with the blade passing frequency whether cavitation occurs or not, while the pulsation intensity increases obviously after cavitation inception. From the first section to the eighth section of volute, the pulsation intensity of impeller outlet decreases gradually. The results are then compared to provide a reference for the optimum design of the anti-cavitation performance of centrifugal pump.

ARTICLE INFO

Keywords:
Centrifugal pump;
Numerical simulation;
Computational fluid dynamics (CFD);
Tongue;
Cavitation;
Blade loading;
Pressure fluctuation

**Corresponding author:*
cwd@ujs.edu.cn
(Cao, W.)

Article history:
Received 18 August 2020
Revised 14 September 2020
Accepted 16 September 2020

1. Introduction

The generation of cavitation can cause severe damage in hydraulic machinery. In liquid flows, the vaporization of liquid is generally due to the local pressure becomes lower than the saturated vapor pressure [1]. Volute pumps are among the most used centrifugal pump types, mainly in mining, petrochemical, and paper industries. Cavitation is a major undesirable phenomenon, which occurs in the operation of centrifugal pumps [2]. The occurrence of cavitation in passages affects the energy change between the wall surface and liquid, which leads to the breakdown of performance, surface erosion, and even the equipment failure [3, 4]. In case of centrifugal pumps, the cavitation inception generally takes place on the suction surface of the blades near their leading edge, and the cavity presents an asymmetrical feature, which is caused by the interaction between the blade and tongue of volute.

On this basis, cavitation in centrifugal pumps have been extensively studied [5-12]. Most studies mainly focused on the cavitation detection in impellers and performance improvement through the application of cavitating flow simulation. However, only a few studies on the cavita-

tion at the tongue of volute have been conducted based on visualization experiment and simulation computation. At overload conditions, flow separation, characterized by unsteady vortex shedding from the tongue, causes the low pressure zone near the tongue. The present study deals with a special case, where cavitation near the tongue of the volute occurs prior to the cavitation at the leading edge of blades. The head drop curve also has a knee shape that head remain constant with the decrease of *NPSH* and rapidly decreases at critical point. In this case the breakdown of performance due to cavitation at the tongue rather than cavitation in impeller. With pressure fluctuation and visualization experiment, and combining numerical simulation, the cavitation structure at the tongue and its influence to the flow field in impeller was investigated. The results were then compared to provide a reference for the optimum design of centrifugal pump.

2. State of the art

The investigation of flow filed in the vicinity of or inside cavitation is complex in spite of remarkable progress on the experimental technique and numerical calculation. R.F. Kunz *et al*. [13] predicted the occurrence and evolution of single airfoil cavitation by using a two-phase flow model based on the Navier-Stokes equation. On this basis, the present study conducted a numerical simulation analysis and research on a centrifugal pump and investigated the anti-cavitation performance. Luo *et al*. [14] compared the cavitation prediction for a centrifugal pump with and without volute casing. Both models predicted the performance deterioration caused by cavitation, while the asymmetrical feature of cavitating flow exists when the calculation domain with volute casing is applied. And the performance deterioration caused by the asymmetrical cavitation is overestimate based on the experiment data. Rudolf *et al*. [15] provide high-speed photographic observation of successive stages of unsteady cavitation at the tongue of the volute of a centrifugal pump. The experiments were carried out at a flow rate above optimal value and at 3 % head drop conditions. The cloud cavitation at the tongue is similar to the one on single hydrofoils. However, only direct visualization was conducted to explain the evolution of cavitation structures at the tongue of centrifugal pump at overload conditions, numerical method was not employed to investigate the cavitation phenomenon at the tongue. To slove the cavitation damage problem near the casing tongue of an afterburner fuel pump, Xue *et al*. [16] investigated the separated flow characteristics and pressure fluctuations around the tongue by large eddy simulations. It is found that at low flow conditions, the fuel backflow from diffuser to the annular chamber triggers serious separation, which lowers the local static pressure to less than zero. The location of the separated vortex is in accord with the cavitation damage core region. Meng *et al*. [17] simulated and analyzed the complex transient cavitation flow patterns inside a centrifugal pump. The cavities in the passages exhibit an obvious life cycle with a frequency corresponding to the impeller rotation frequency under off-design conditions. The asymmetric cavitation in associated with the uneven pressure distribution on volute and impeller-tongue interaction. Dular *et al*. [18] employed the PIV-LIF method to obtain the velocity field inside and outside the vapour cavity around two hydrofoils. On the basis of the captured images of vapor structures, it can been seen that the cavitation behaves dynamically at the front wall. The backflow causes the separation of cavitation cloud and the vortex remains present inside the separated cloud. The development of unsteady cavitation on impeller blades resembles that on a single hydrofoil. However, in the case of a centrifugal pump, the interaction between the impeller and the volute tongue strongly affects cavitation evolution due to the periodically variation of the flow fields in passages. Limbach *et al*. [19, 20] conducted the numerical calculation and experimental work on a low-specific-speed centrifugal pump. It is observed that the Net positive suction head (NPSH) rises toward overload due to incidence, flow separation, and vapor zones at the volute tongue. The numerical simulation has been performed by Micha *et al*. [21] to study the effect of tip-vortex cavitation in a centrifugal pump and its result on the change in nuclei size. The size of bubble nuclei significantly affect the incipient of cavitation and unsteady pressure distribution in passages and the suction surface of the impeller leads to separation and re-circulation at off-design condition which in turn influences the onset of cavitation at the leading edge of the blade. Ahmed *et al*. [22] analyzed the vibration signal in both time and frequency domains to detect and

diagnose the cavitation phenomenon within a centrifugal pump. With various flow rates and rotational speed, the signals presented similar statistical features and revealed that using low-frequency was sensitive to predict cavitation in the pump. By means of unsteady numerical computation, Tang *et al*. [23] found that the blade passing frequency is the dominant frequency of the pressure fluctuations in the casing except the vicinity of the volute tongue for all operating conditions, and the dominant one near the volute tongue is the blade passing frequency at the design point and 0~0.5 times the blade passing frequency at other off-design points. Dönmez *et al*. [24] and Tao *et al*. [25] investigated the influence of geometric parameters of blade inlet on cavitation phenomenon of the centrifugal pump. Cavitation performance of pump is excessively affected by both blade inlet angle and blade leading-edge shape. Increasing hub blade angle has slightly negative effect on cavitation performance of the pump, and the round and ellipse leading-edge impellers have higher inception cavitation coefficient than the ones with blunt or sharp leading-edge. Alex *et al*. [26] compiled an overview on the effect of cavitation in the performance of centrifugal pump. They took account of parameters such as blade numbers, blade angle, inlet flow angle, flow rates, and inlet and outlet pressure. These parameters all have influence on the cavitation performance, however the casing type or the tongue shape were not considered

Above research results indicate that the evolution of cavitation causes the performance deterioration of centrifugal pump and the development of cavitation cloud in passages usually emerges at the suction side of blade leading edge. During the experiment, the pump was operating at overload flow rate and cavitation condition leading to 3 % head drop. Detailed observations of cavity evolution near the tongue of casing were made when no obvious cavitation occurs within the impeller. On the basis of numerical simulation and hydraulic testing, this study explored cavitation structure and flow field in the vicinity of the tongue of the volute casing to provide guidance for the optimization design of centrifugal pumps.

3. Materials and methods

3.1 Design of test stand

The closed testbed is shown in Fig. 1. The pressure fluctuation and cavitation at tongue downstream experiments were conducted on the testbed, except for measuring the external characteristics of the pump model under different flow rates. In Fig.1, impeller and volute were prepared with PMMA. The testbed was equipped with a pressure transmitter, a turbine flowmeter, and a high-frequency pressure sensor for the effective measurement of testing parameters: turn frequency (n), spindle torque (T), mass flow (Q), pressure fluctuation, and inlet and outlet pressures of the pump model (p_{in} and p_{out}). Design parameters of the model pump are shown in Table 1.

Table 1 Design parameters

Q_d(m³/h)	10
H(m)	11
n(r/min)	1450
P(kW)	3
Impeller diameter D_2(mm)	192
Impeller inlet diameter D_1(mm)	54
Impeller hub diameter d_h(mm)	20
Impeller width b_2(mm)	5
Blade outlet angle β_2	27.5

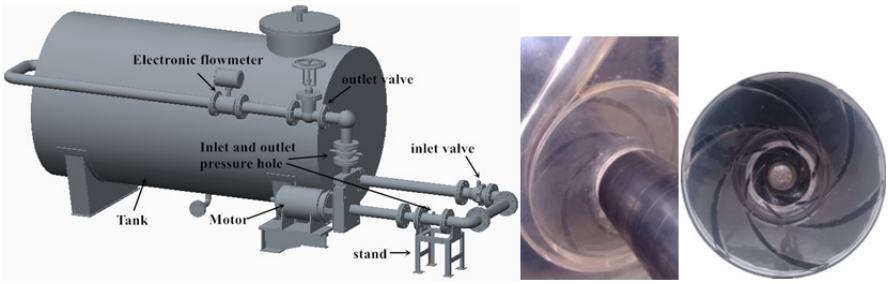

Fig. 1 Three-dimensional schematic of the test stand

3.2 Pressure fluctuation test

The test field of pressure fluctuation is shown in Fig. 2. The overall structure of the testbed is shown in Fig. 2(a). Under the assistance of a high-frequency dynamic pressure sensor, the pressure fluctuation characteristics at the tongue downstream were monitored with a HSJ2010 hydraulic machinery comprehensive tester developed by Huazhong University of Science and Technology. The distributions of pressure fluctuation measurement points are shown in Figs. 2(b) and 2(c). The sampling frequency and sampling time of test data were set to 8,700 Hz and 60 s, respectively.

(a) (b) (c)

Fig. 2 The pressure fluctuation testing station

3.3 High-speed photography experiments

The experimental apparatus for high-speed photography is shown in Fig. 3. The positions in Fig. 3 show the locations of the light source and CCD camera in the test. The capture frequency was set to 500 images/s, and the pixel depth of images was set to 8 bits due to the low revolution speed of the test pump. The pixels of the obtained image were 860×1,280. The arrow in Fig. 3 shows the shooting direction of the camera and the incidence angle of light source to decrease the interferences of the reflected light.

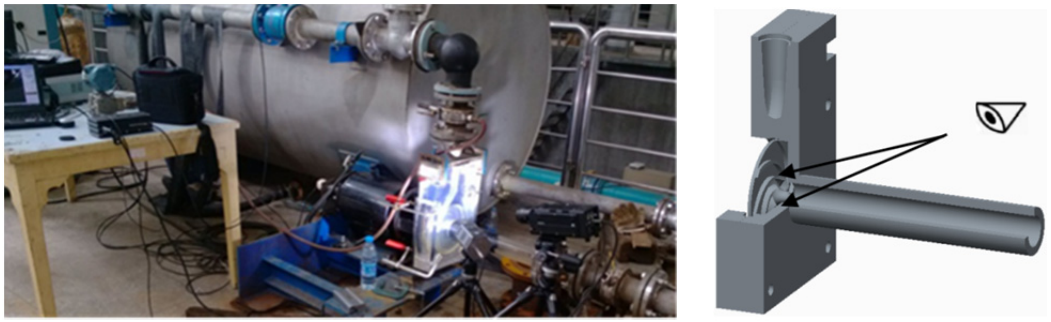

Fig. 3 High-speed photographic experiment device

3.4 Analysis of the test results

The overall external characteristics of the pump are shown in Fig. 4. The flow head curve under non-cavitation is shown in Fig. 4(a), and the *NPSH-H* curve is shown in Fig. 4(b) when $Q/Q_d = 1.52$. With the reduction in *NPSH*, no evident cavitation is found at the back of the impeller inlet. However, evident cloudy cavitation is detected close to the tongue near the flow measuring points.

$$NPSH = \frac{p_{in} - p_v}{\rho g} + \frac{v_{in}^2}{2g} \tag{1}$$

where p_{in} is the static pressure at the impeller inlet, p_v is the saturated vapor pressure, taken as 3574 Pa, v_{in} is the absolute velocity at the impeller inlet.

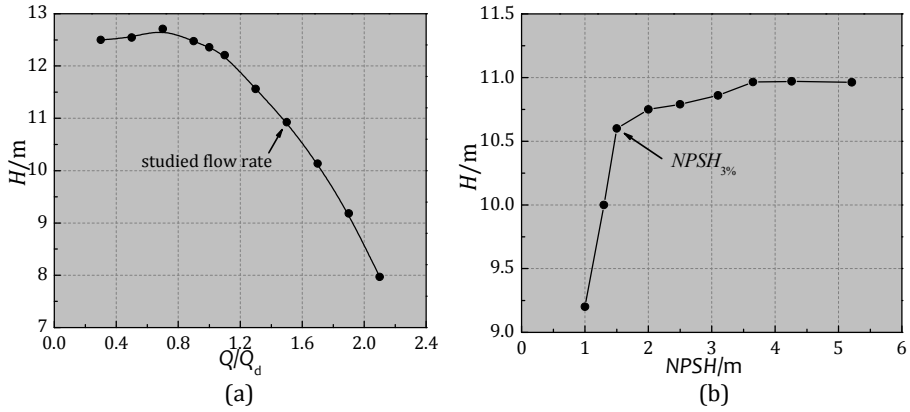

Fig. 4 External characteristic curve of the model pump

The pressure fluctuation in rotating hydraulic machinery can be divided into three types, namely, random pressure, blade multifrequency, and axial multifrequency fluctuations. The random pressure fluctuation is induced by cavitation, eddies, and unsteady secondary flows. It is similar with white noise on the spectrum. The blade frequency fluctuation has a multiple relation with blade passing frequency and is related to rotor-stator interaction. The shaft frequency fluctuation is related to mechanical speed. In this study, the rotational speed of the centrifugal pump was 1,450 rpm. The patterns of time and frequency domains at $Q/Q_d = 1.52$ and $NPSH_{3\%} = 1.5$ m are shown in Fig. 5. The domain pressure fluctuation in the flow field at the volute downstream is mainly blade passing frequency.

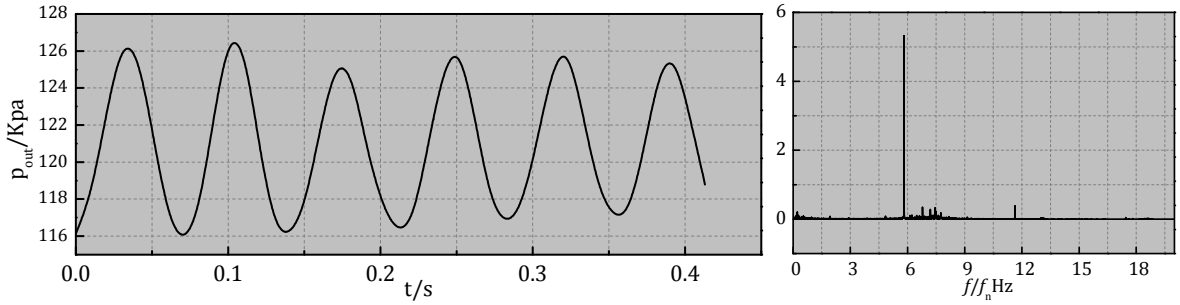

Fig. 5 Time-domain and frequency-domain of the pressure fluctuation in monitoring point

The high-speed photography results at the tongue of the pump model at $Q/Q_d = 1.52$ are shown in Fig. 6. Figure 6 shows that: a) A large cavitation structure is developed at the leading edge of the tongue when the blade leaves the observation range, b)The cavitation cloud at the leading edge of the tongue develops quickly and sheds when the next blade appears in the visual frame, c) The flow regime deteriorates, and many bubbles begin to develop at the leading edge when the blade approaches the tongue, d) The cavitation cloud at the tongue tends to attach on the cavities when the blade is close to the tongue position, e) The cavitation cloud rapidly blocks the flow passage near the tongue because the blade leaves the tongue and moves to the downstream areas, significantly influencing the energy transmission in the volute.

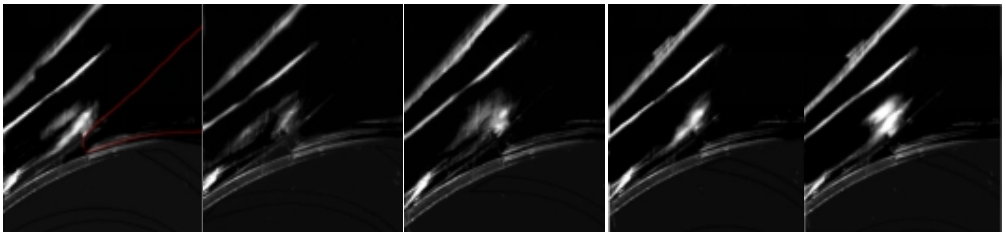

Fig. 6 Cavitation evolution at the volute tongue

4. Result analysis and discussion

4.1 Method of numerical simulation

Time-averaged N-S equations were utilized as the basic governing equations in the single-phase computation. The SST k-ω turbulence model was selected for 3D turbulence numerical simulation because it considers the transmission of turbulence shear stress and can accurately predict the initial position and results of fluid separation under turbulent negative-pressure gradient. The transport behavior was obtained using the eddy viscosity equation containing the limiting quantity

$$v_t = \frac{\alpha_1 k}{\max(\alpha_1 \omega S F_2)} \tag{2}$$

where v_t denotes dynamic viscosity, α_1 is a constant taken as 5/9, k is turbulent kinetic energy, ω is turbulence frequency, F_2 is mixing function that constrains the limiting quantity in the boundary layer, and S is the invariant measure of shear rate.

A homogeneous model was used in the vapor-liquid two-phase flow field. The Zwart equation based on the Rayleigh-Plesset formula was used to analyze the generation and collapse of cavitation bubbles and the mass transfer in the fluid. The evolution process of cavitation bubbles is given as

$$R_B \frac{\mathrm{d}^2 R_B}{\mathrm{d}t^2} + \frac{3}{2}\left(\frac{\mathrm{d}R_B}{\mathrm{d}t}\right)^2 + \frac{2\sigma}{\rho_f R_B} = \frac{p_v - p}{\rho_f} \tag{3}$$

where R_B is the radius of bubble, p_v is the pressure inside the bubble, p is the pressure of the fluid around bubble, ρ_f is the density of the fluid, and σ is the surface tension of the interface between the fluid and bubble.

ANSYS ICEM was used to generate high-quality hexahedral meshes in the computational domains of the model pump. Fifteen mesh layers were added to each boundary while guaranteeing that the distribution of blocks was accordance with the flow regime in the computational domains to ensure the accuracy of the numerical simulation in the near-wall zone. Mesh independence was applied under the design condition to guarantee calculation accuracy and improve calculation efficiency. When the grid number exceeded 2.6 million, the change in the pump head was within 1 %. Thus, the grid number was determined. Fig. 7 shows a 3D model of the computational domain, and Fig. 8 shows a schematic of the computation meshes. The left side presents the cross-section mesh of the impeller and volute, and the right side shows partial enlargement of the mesh at the inlet and outlet of blade.

Steady-stage computation of multiple working conditions was performed with different inlet attack angles by using ANSYS-CFX 16.0 software. Given that *NPSH* is closely related to the pressure at the pump inlet, the total pressure in the inlet and the mass flow in the outlet were used for the computational domain. The calculations for non-cavitation simulation were used as the initial results for the cavitation simulation to reduce the calculation time.

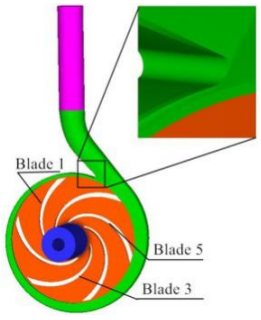

Fig. 7 Computational domain

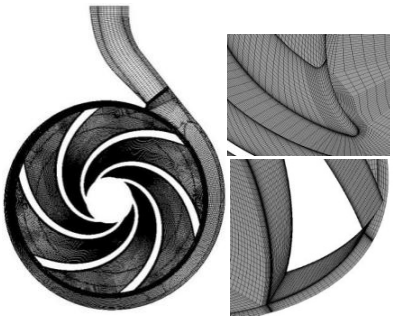

Fig 8 Schematic of the mesh

4.2 Numerical simulation results and analysis

The one-sixth cycle numerical simulation results of cavitation at the tongue at $Q/Q_d = 1.52$ are shown in Fig. 9. The short tongue adopted in this study differs significantly from ordinary airfoil profile but its cavitation structure has great similarities to the attachment and shedding of cavities on single airfoil. The inlet speed and Strouhal number are the main factors influencing periodic cavitation formation and shedding on single airfoil. For the cavitation at the tongue , the development of cavitation is influenced by the interaction changes in pressure gradients between the pressure surface (PS) and suction surface (SS) of blades and the unsteady changes in flow field near the leading edge of the tongue caused by jet wake at the impeller outlet.

As shown in Fig. 9(a), the tongue at 0 T is in the middle of flow passage. At this moment, a relatively large cavitation cloud occurs at the leading edge of the tongue. At 1/4 T, the cavitation cloud develops quickly at the tongue and sheds when the next blade approaches the tongue. At 1/2 T, the cavitation cloud gradually moves toward the tongue downstream when the blade approaches the tongue. The cavitation cloud separates in the high-pressure zone at the tongue downstream, thereby decreasing the area of low-pressure zone. At 3/4 T, the blade is located at the tongue, and a newly attached cavitation emerges at the tongue. The previous cavitation cloud breaks quickly and then moves downward. The flow regime in the volute deteriorates, and cavitation wake occurs at the downstream close to the volute outlet. Thus, the low-pressure zone is expanded. At 1 T, the blade leaves the tongue, and the cavitation cloud develops at the leading edge of the tongue, exerting the evident blocking effect of the flow passage. With the shedding of cavities, the actual flow area close to the tongue increases suddenly, thereby causing great energy losses in the volute.

The velocity diagram for the middle section of the pump in a single cycle is shown in Fig. 9(b). Uniform relative rates are found on the middle stream surface of the blade, and a local high-pressure zone is found at the blade outlet close to the tongue. At overload conditions, serious separation occurs at the tongue. The negative pressure fluctuation caused by separation and transition can trigger the initiation of cavitation. Separated unsteady eddies are formed near the tongue, which are the vibration and noise sources. At 0 T, a low-rate backflow zone that occupies approximately one-half of the flow passage is formed at the leading edge and tongue downstream, significantly blocking the flow passage. The cavitation cloud develops quickly and squeezes the actual flow area. At 1/4 and 1/2 T, the blocked passage is released partially with the shedding of cavities. The low-rate backflow zone shrinks, and the eddies move downward. The flow field near the tongue is divided into backflow and mainstream zones. At 3/4 T, the blade outlet is close to the tongue, and the eddy center moves downward. The previous cavitation cloud moves downward to form a cavitation wake. At 1 T, the blade leaves the tongue, and a new cavitation cloud emerges at the leading edge of the tongue.

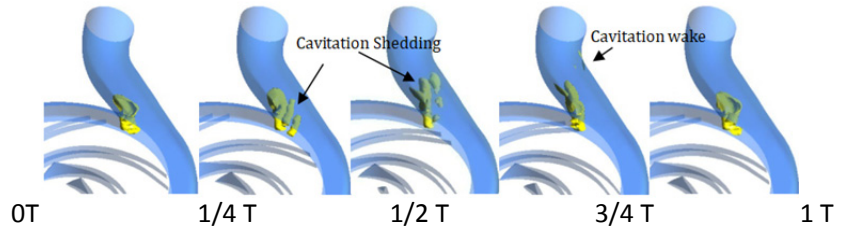

(a) Cavitation evolution at the tongue

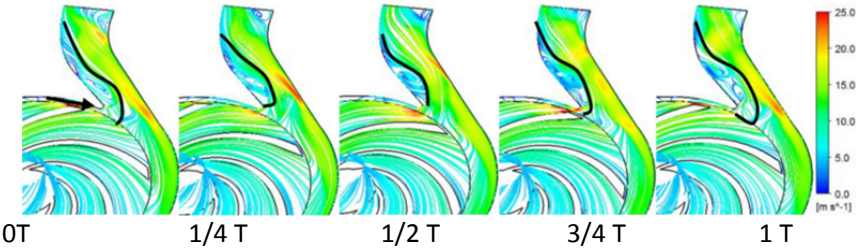

(b) Velocity distribution on the cross section of the pump

Fig. 9 Flow field at $Q/Q_d = 1.52$

A centrifugal pump with a helical pumping chamber can generate a radial force that acts on the impeller during operation. Thus, the axis bears alternating stresses and generates a directed deflection. The pressure in the chamber of the centrifugal pump continuously changes due to the interference by the impeller and the tongue of the volute, thereby generating unsteady radial forces. The existence of cavitation may affect the radial forces. The vector diagram of radial force distribution on the impeller in a single cycle under different flow rates is shown in Fig. 10. Cavitation occurs at the impeller inlet when Q/Q_d = 1.3 and 1.52. However, the radial force distributions at the critical cavitation state are basically consistent under three working conditions. The radial force distribution is related to the number of blades and is in hexagonal star distribution. This condition is caused by the interference of the impeller and the volute. At Q/Q_d = 1.3, the vector diagrams under critical cavitation and non-cavitation conditions are close. At Q/Q_d = 1.52 and 1.73, the radial forces produce alternating stresses under cavitation conditions when the blade sweeps the separation tongue.

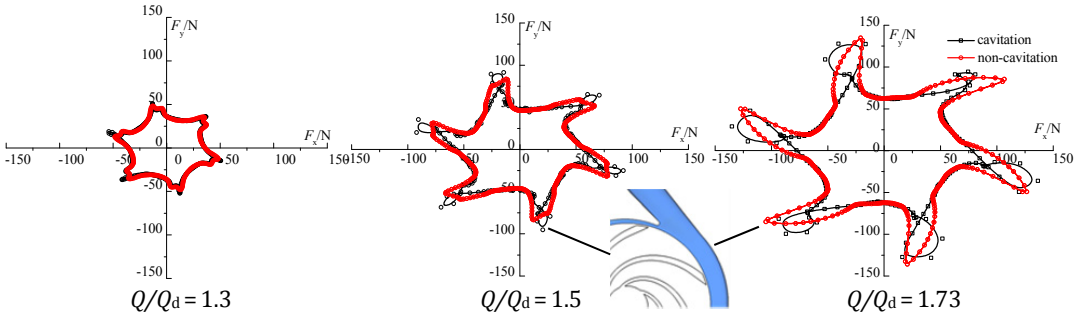

Fig. 10 Distribution of radical force

The secondary flows and "jet wake" phenomenon are caused by the high-speed rotation of the impeller, interference between the impeller and the volute, and the viscosity of fluid due to the spatial asymmetric structure of the centrifugal pump. The internal flow field presents complicated unsteady characteristics that may cause pressure fluctuation. The circumferential pressure fluctuation of the volute and pressure fluctuation near the tongue are influenced and present different characteristics when cavitation emerges at the tongue. The monitoring points of pressure fluctuation in the volute are shown in Fig. 11.

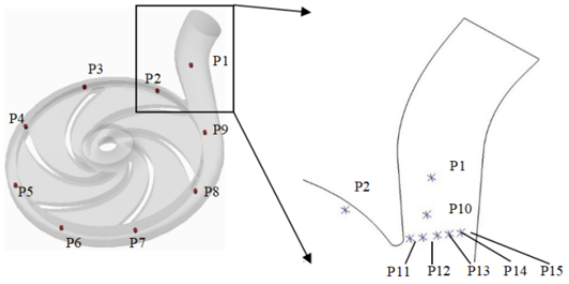

Fig. 11 Monitoring points of pressure fluctuation

The pressure amplitude of pressure pulsation in the volute is characterized, and the influences of the static pressure of monitoring points on pressure fluctuation are eliminated. The strength of pressure fluctuation is expressed as pressure coefficient C_p

$$C_p = \frac{p-\overline{p}}{\frac{1}{2}\rho U^2} \tag{4}$$

where p is the instantaneous pressure value at the monitoring points, and $\overline{p}$ is the mean pressure of monitoring points in the investigated cycle.

The time domain of monitoring points P1-P9 when Q/Q_d = 1.3, 1.52, and 1.73 is shown in Fig. 12. The pressure fluctuation intensity increases significantly with the increase of flow rate. Although the number of wave peaks at different monitoring points in a single cycle is equal to the number of blades, the regularity in a single cycle weakens with the increase of flow rate. At Q/Q_d =

1.3, the pressure fluctuation at different monitoring points shows evident periodic fluctuation laws. The fluctuation amplitudes at different monitoring points are close, except for the monitoring points at the downstream of the tongue. Considering that all monitoring points are close to the flow field at the impeller outlet, the pressure fluctuation is caused by the jet-wake structure at the passage outlet of the impeller, and the fluctuation amplitudes are similar. At $Q/Q_d = 1.73$, irregular wave peaks are found, indicating the occurrence of serious cavitation close to the tongue. Therefore, the flow field becomes extremely disordered.

The multiplication of rotating frequency is defined as

$$NF = \frac{60F}{n} = \frac{F}{F_n} \tag{5}$$

where F is the practical frequency after Fourier transform, n is the rotating speed of the impeller, and F_n is the rotating frequency under the corresponding rotating speed.

As shown in Fig. 13, the excitation frequency at different monitoring points is the blade passing frequency under different flow rates. The shaft frequency and other low-frequency and high-frequency bands have small amplitudes. This finding reveals that the pressure fluctuation caused by the "jet wake" flow structure under high flow rate is the main excitation frequency. With the increase in flow rate, the pressure fluctuation strength increases significantly. In particular, a magnitude of jumps of pulsation strength is found after the cavitation occurs at the tongue. At $Q/Q_d = 1.3$, the pressure fluctuation is weak. The main excitation frequency first decreases and then increases from the first to the eighth sections. The pressure fluctuation strength declines as the monitoring point moves away from the tongue. At $Q/Q_d = 1.52$ and 1.73, the cavitation in the volute becomes evident, and the pressure fluctuation in the volute shows different laws. The pressure fluctuation at the downstream of the tongue is lower than that at the impeller outlet. The fluctuation strength at the impeller outlet decreases gradually from the first to the eighth sections.

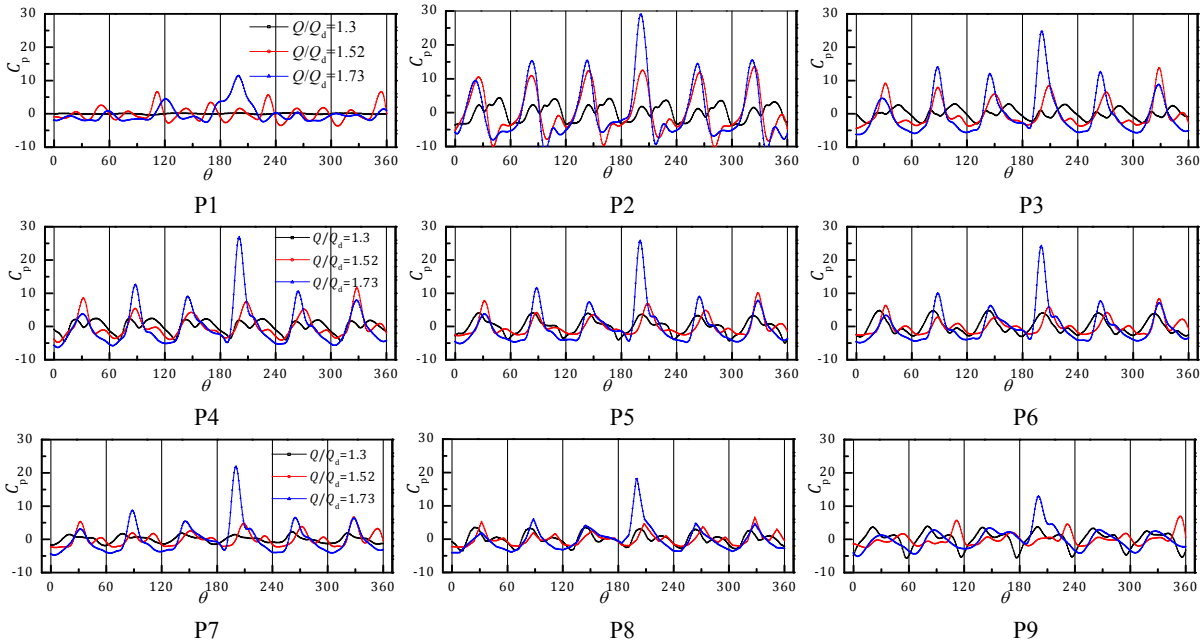

Fig. 12 Pressure fluctuation of monitoring points around the impeller outlet

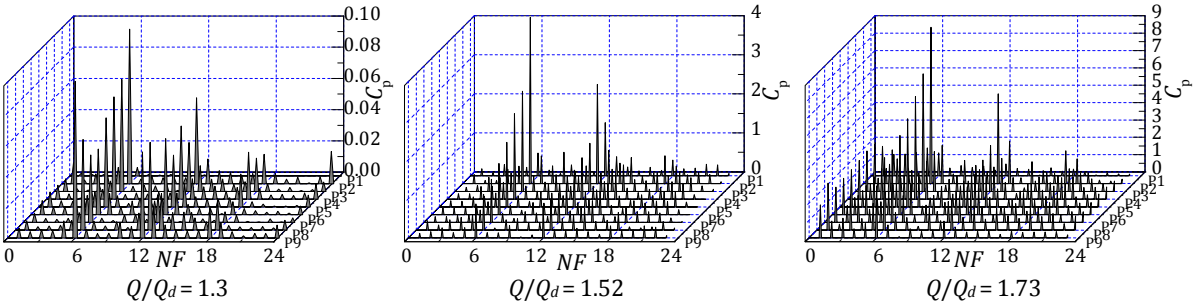

Fig. 13 Frequency domain of pressure fluctuation

The time domains of pressure fluctuation at P10-P15 are shown in Fig. 14. The pressure fluctuation has six wave peaks under different working conditions, and the pressure fluctuation at different monitoring points is caused by the interference of the tongue. The pressure fluctuation strength increases with the increase of flow rate. The fluctuation strength weakens when the distance between the monitoring point and the tongue increases. The influence of the tongue on pressure fluctuation and the influence of jet-wake structure at the impeller outlet decline when the monitoring point approaches the wall surface facing the tongue. The pressure fluctuation strength without cavitation close to the tongue at $Q/Q_d = 1.3$ is significantly lower than that with cavitation at the tongue at $Q/Q_d = 1.52$ and 1.73. This finding reflects that the unsteady flow at the tongue is complicated, and the changes in pressure distribution are intense after the occurrence of cavitation. At actual operation, these conditions may trigger serious vibration noises, thereby influencing the stable operation of the pump.

The frequency domains of pressure fluctuations at different monitoring points close to the tongue under different working conditions are shown in Fig. 15. The dominant frequency under working conditions is the blade passing frequency. The rapid increase in dominant frequency amplitude caused by cavitation reflects the influences of cavitation development on the pressure fluctuation strength close to the tongue. The pressure fluctuation at the downstream monitoring point P1 is 0.41 of the dominant frequency amplitude under non-cavitation condition. However, it increases to 2.12 and 3.84 when $Q/Q_d = 1.52$ and $Q/Q_d = 1.73$, respectively. A strong pressure fluctuation may be found at the downstream position of the tongue due to the development and breakage of cavities. In accordance with the changes in dominant frequency amplitude under different working conditions, the pressure fluctuation intensity declines gradually when the monitoring point approaches the wall surface facing the separation tongue.

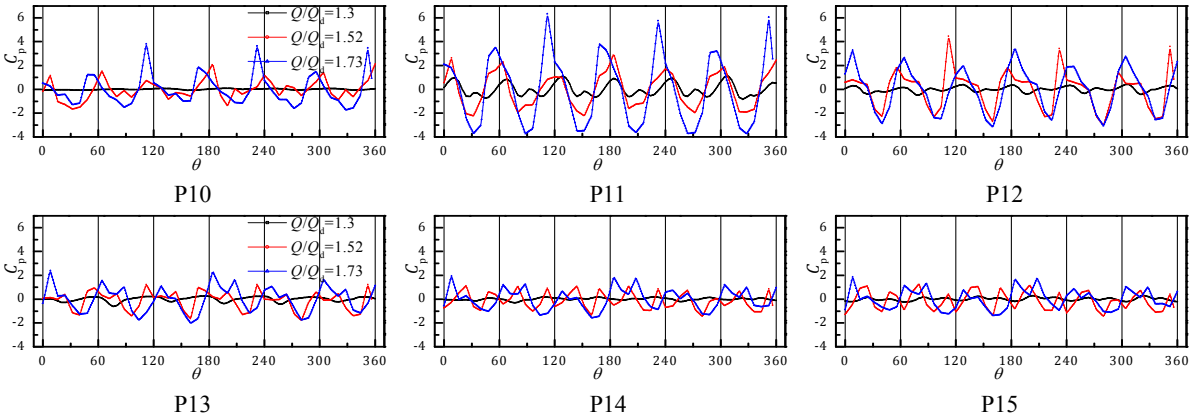

Fig. 14 Pressure fluctuation near the tongue

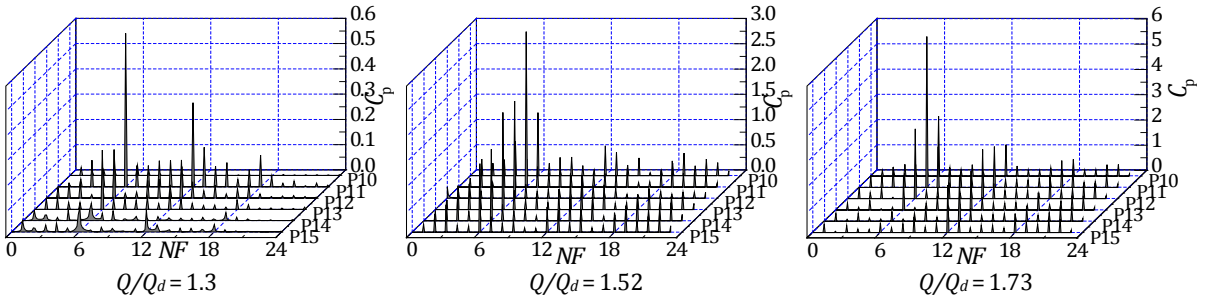

Fig. 15 Frequency domain of pressure fluctuation of monitoring points near the tongue

5. Conclusion

In this study, an attempt is made to investigate the cavitation at the tongue of centrifugal pump at overload conditions. By means of numerical computation and visualization measurement, unsteady flow structures in cavitation zone were studied to associate with blade loading and pressure fluctuation. From the present research following conclusions can be drawn:

- As the increase of flow rate, the shedding of the separated vortex lowers the static pressure near the tongue. And the flow separation at the tongue brings dramatic pressure fluctuation and strong shearing vortex which induce cavitation.
- At overload conditions, higher radical velocity and deviation of relative flow angle contribute to periodical variation of flow field near the tongue, which results in periodical cavitation evolution. Thus, the frequency of the cavitation cloud shedding is equal to the blade passing frequency.
- Cavitation at the tongue not only enhances the pressure fluctuation in volute, but also affects the blade loading distribution: The pressure pulsation in the volute is consistent with the blade passing frequency whether cavitation occurs or not, while the pulsation intensity increases obviously after cavitation inception. From the first section to the eighth section of volute, the pulsation intensity of impeller outlet decreases gradually.

The study showed that it is possible that the head drop at overload conditions is caused by the appearance of cavitation at the tongue of volute, which may provide guidance for the optimization of the anti-cavitation performance of centrifugal pump. In future, more accurate visualization measurement and vibration experiment can be conducted to investigate the cavitation phenomenon at the tongue of casing.

Acknowledgement

This research was funded by the National Key R&D Program of China (2018YFC0810506) and the Key R&D Program of Zhenjiang (SH2017049).

References

[1] Brennen, C.E. (2011). *Hydrodynamics of Pumps*, Cambridge University Press, Cambridge, United Kingdom, doi: 10.1017/CBO9780511976728.
[2] Franc, J.-P., Michel, J.-M. (2005). *Fundamentals of cavitation*, Springer, New York, USA, doi: 10.1007/1-4020-2233-6.
[3] Širok, B., Dular, M., Hočevar, M., Novak, M., Stoffel, B., Ludwig, G., Bachert, B. (2002). The influence of cavitation structures on the erosion of a symmetrical hydrofoil in a cavitation tunnel, *Strojniški Vestnik – Journal of Mechanical Engineering*, Vol. 48, No. 7, 368-378.
[4] Wang, S.-L., Tan, L., Wang, Y.-C. (2013). Characteristics of transient cavitation flow and pressure fluctuation for a centrifugal pump, *Journal of Vibration and Shock*, Vol. 32, No. 22, 168-173, doi: 10.13465/j.cnki.jvs.2013.22.024.
[5] Bilus, I., Predin, A. (2009). Numerical and experimental approach to cavitation surge obstruction in water pump, *International Journal of Numerical Methods for Heat & Fluid Flow*, Vol. 19, No. 7, 818-834, doi: 10.1108/09615530910984091.
[6] Lu, J., Yuan, S., Ren, X., Liu, Y., Si, Q. (2015). Investigation of instabilities of cavitation at low flow rate of centrifugal pump, *Transactions of the Chinese Society for Agricultural Machinery*, Vol. 46, No. 8, 54-58, doi: 10.6041/j.issn.1000-1298.2015.08.009.

[7] Čudina, M., Prezelj, J., Černetič, J. (2012). Use of noise and vibration spectra to detection cavitation in kinetic pumps, In: *Proceedings of the 8th International Symposium on Cavitation,* Singapore, 978-971, doi: 10.3850/978-981-07-2826-7_172.
[8] Lu, Z., He, X., Wang, C. (2018). Influencing factors of self-priming time of multistage self-priming centrifugal pump, *DYNA – Ingeniería e Industria*, Vol. 93, No. 6, 630-635, doi: 10.6036/8930.
[9] Ključanin, D., Manđuka, A. (2019). The cantilever beams analysis by the means of the first-order shear deformation and the Euler-Bernoulli theory, *Tehnički Glasnik,* Vol. 13, No. 1, 63-67, doi: 10.31803/tg-20180802210608.
[10] Luo, X., Zhang, Y., Peng, J., Xu, H. (2008). Effect of impeller inlet geometry on centrifugal pump cavitation performance, *Journal of Tsinghua University (Science and Technology)*, Vol. 48, No. 5, 836-839, doi: 10.3321/j.issn:1000-0054.2008.05.019.
[11] Castorani, V., Landi, D., Mandolini, M., Germani, M. (2019). CFD simulations of filter houses for power plant gas turbine: Evaluation of differences between 2D and 3D models, *DYNA – Ingeniería e Industria,* Vol. 94, 145-149, doi: 10.6036/8901.
[12] Blecich, P., Senčić, T., Wolf, I., Bonefačić, I. (2018). Numerical investigation of heat and mass transfer inside a wet cooling tower, *Tehnički Glasnik,* Vol. 12, No. 3, 131-138, doi: 10.31803/tg-20171017145907.
[13] Kunz, R.F., Boger, D.A., Stinebring, D.R., Chyczewski, T.S., Lindau, J.W., Gibeling, H.J., Venkateswaran, S., Govindan, T.R. (2000). A preconditioned Navier–Stokes method for two-phase flows with application to cavitation prediction, *Computers & Fluids,* Vol. 29, No. 8, 849-875, doi: 10.1016/s0045-7930(99)00039-0.
[14] Luo, X., Wei, W., Ji, B., Pan, Z., Zhou, W., Xu, H. (2013). Comparison of cavitation prediction for a centrifugal pump with or without volute casing, *Journal of Mechanical Science and Technology*, Vol. 27, No. 6, 1643-1648, doi: 10.1007/s12206-013-0411-5.
[15] Bachert, R., Stoffel, B., Dular, M. (2010). Unsteady cavitation at the tongue of the volute of a centrifugal pump, *Journal of Fluids Engineering*, Vol. 132, No. 6, Article No. 061301, doi: 10.1115/1.4001570.
[16] Xue, M., Park, Y. (2012). Large eddy simulations of separated flow at the casing tongue of an afterburner fuel pump, *Journal of Tsinghua University (Science and Technology)*, Vol. 52, No. 11, 1638-1642, doi: 10.16511/j.cnki.qhdxxb.2012.11.023.
[17] Meng, L., He, M., Zhou, L., Yang, J., Wang, Z., Karney, B. (2016). Influence of impeller-tongue interaction on the unsteady cavitation behavior in a centrifugal pump, *Engineering Computations*, Vol. 33, No. 1, 171-183, doi: 10.1108/EC-09-2014-0179.
[18] Dular, M., Širok, B., Bachert, R., Stoffel, B. (2005). Transient simulation, visualization and PIV-LIF measurements of the cavitation on different hydrofoil configurations, *Strojniški Vestnik – Journal of Mechanical Engineering,* Vol. 51, No. 1, 13-27.
[19] Limbach, P., Kimoto, M., Deimel, C., Skoda, R. (2014). Numerical 3D simulation of the cavitating flow in a centrifugal pump with low specific speed and evaluation of the suction head, In: *Proceedings of the ASME Turbo Expo 2014: Turbine Technical Conference and Exposition. Volume 2D: Turbomachinery,* Düsseldorf, Germany, 16-20, doi: 10.1115/GT2014-26089.
[20] Limbach, P., Skoda, R. (2017). Numerical and experimental analysis of cavitating flow in a low specific speed centrifugal pump with different surface roughness, *Journal of Fluids Engineering*, Vol. 139, No. 10, Article No. 101201, doi: 10.1115/1.4036673.
[21] Micha Premkumar, T., Sathish Babu, R., Vinoth Kumar, M., Hariram, V., Seralathan, S. (2019). Numerical simulation of hydrodynamic cavitation in centrifugal pump, *International Journal of Innovative Technology and Exploring Engineering*, Vol. 8, No. 11, 2689-2693, doi: 10.35940/ijitee.k2140.0981119.
[22] Al-Obaidi, A.R. (2019). Investigation of effect of pump rotational speed on performance and detection of cavitation within a centrifugal pump using vibration analysis, *Heliyon*, Vol. 5, No. 6, Article No. E01910, doi: 10.1016/j.heliyon.2019.e01910.
[23] Tang, X., Zou, M., Wang, F., Li, X., Shi, X. (2017). Comprehensive numerical investigations of unsteady internal flows and cavitation characteristics in double-suction centrifugal pump, *Mathematical Problems in Engineering*, Vol. 2017, Article ID 5013826, doi: 10.1155/2017/5013826.
[24] Dönmez, A.H., Yumurtacı, Z., Kavurmacıoğlu, L. (2018). The effect of inlet blade angle variation on cavitation performance of a centrifugal pump: A parametric study, *Journal of Fluids Engineering*, Vol. 141, No. 2, Article No. 021101, doi: 10.1115/1.4040557.
[25] Tao, R., Xiao, R., Wang, Z. (2018). Influence of blade leading-edge shape on cavitation in a centrifugal pump impeller, *Energies*, Vol. 11, No. 10, Article No. 2588, doi: 10.3390/en11102588.
[26] George, A., Muthu, P. (2015). Review on effects of cavitation in the performance of centrifugal pump, *International Journal of Advance Engineering and Research Development*, Vol. 2, No. 11, 298-303, doi: 10.21090/ijaerd.021148.